Designing, building and testing a UV photouncaging system to study the development of the auditory brainstem

Designing, building and testing a UV photouncaging system to study the development of the auditory brainstem

By Arjun Kathir, B.Eng.

A Thesis submitted to the School of Graduate Studies in Partial Fulfillment of the Requirements for the Degree of Master's

McMaster University

Master's of Science (2018)

neuroscience

McMaster University

Hamilton, ON

Title: Designing, Building and Testing a UV Photouncaging system to Study the Development of the Auditory Brainstem

Author: Arjun Kathir, B. Eng. (McMaster University)

Supervisor: Dr.Deda C. Gillespie

Number of pages:

ABSTRACT

In mammals, sound localization along the azimuth is computed in part in the lateral superior olive (LSO), a binaural nucleus in the brainstem. Information about the location of the sound source is derived from differences in sound intensity at the two ears, the Interaural Level Difference (ILD). Within each LSO, principal cells compute ILDs by integrating an excitatory input carrying intensity information from the ipsilateral ear with an inhibitory input carrying intensity information from the contralateral ear. This computation requires that the phenotypically distinct inputs onto individual LSO cells be matched for sound frequency. The process of 'aligning' and refining the inputs for frequency information occurs during the first few postnatal weeks in rats, through modifications of synapse strength and cell morphology. Our lab studies the distribution, and re-distribution, of these converging inputs during the early period of circuit refinement.

A common strategy for examining spatial distribution of synapses is through anatomical techniques, including for example immunohistological methods for localizing specific synaptic proteins. Ultimately, however, we need to understand how synapse position affects the functional response. Asking this kind of question requires the ability to stimulate individual synapses while recording from dendrite or cell body, an approach for which we use laser scanning photostimulation (LSPS). I designed two LSPS systems in order to stimulate the post-synaptic sites of excitatory or inhibitory inputs on LSO principal neurons while recording at the cell body using whole-cell patch clamp. I researched many optical designs and technologies when fine-tuning my design. My designs and initial groundwork will help a future lab member finish one or both of the LSPS designs.

ACKNOWLEDGEMENTS

I would like to thank my supervisor Dr. Deda Gillespie. Deda has always encouraged me to bridge the gap between engineers and scientists. Deda always challenges me to understand the biological question which my project aims to answer. She encouraged me to be more self-motivated and active in my learning. I would also like to thank Dr. Fang and Dr. Goldreich for serving on my supervisory committee. They provided me with the guidance I needed during my time as a graduate student. I would like to thank the members of Dr. Fang's Lab. I would like to thank Dr. Anthony Tsikouras and Nehad Hirmiz for their invaluable help with the optical design, and Morgan Richards for his software expertise. I would also like to thank all the members of the Gillespie lab.

I am thankful for the friends and family that helped me through the difficult times. They are always there to cheer me up and motivate me to push forward.

Contents

List of Figures

List of Tables

LIST OF ALL ABBREVIATIONS AND SYMBOLS

AOD	acousto-optical deflector
ATP	adenosine triphosphate
AVCN	anteroventral cochlear nuceus
DMD	digital micromirror device
FOV	field of view
GABA	gamma-aminobutyric acid
Galvo	galvanometer-based scanner
IHC	inner hair cell
IR	infrared
ILD	interaural level difference
LSO	lateral superior olive
LSPS	laser scanning photostimulation
MNTB	medial nucleus of the trapezoid body
NDF	neutral density filter
NIR	near-infrared
OD	optical density
P3	post-natal day 3 (etc.)
res	resolution
SOC	superior olivary complex
UI	uncaging index
UV	ultraviolet

DECLARATION OF ACHIEVEMENT

I designed an optical system to be used for ultra violet through-the-lens photouncaging with the aid of Dr. Deda Gillespie and Dr. Anthony Tsikouras. I independently researched all the components necessary for the optical system. I ensured compatibility of the components through mathematical calculations. I also designed the optical system to be used for near-infrared through-the-lens photouncaging with the aid of Dr. Deda Gillespie. This includes independently researching the parts and determining their compatibility.

1 General Introduction

1.1 Motivation

Studying neural activity at a circuit level is important for fully understanding neural development. A neural circuit is a network of neurons that work together to process specific information. The interconnectivity of these neurons determines the circuit's function. As with an electrical circuit, to monitor the connectivity of a neural circuit requires recording from at least one neuron in the circuit. Where this recording electrode is placed usually depends on the question being answered. Often, neurophysiologists will artificially stimulate an upstream cell in the circuit and record from another cell downstream. When studying circuit connectivity, it is essential that the appropriate recording and stimulating method chosen.

One powerful technique for measuring circuit connectivity is patch-clamp recording. Circuit connectivity can be measured by recording the current from the cell body using whole-cell patch clamp. Patch-clamp recording allows us to measure electrical activity at the cell membrane with high temporal resolution. These recordings are made after stimulating the circuit at a point upstream to the recording site. With the improvements in optical stimulation methods, photostimulation can be done at near-diffraction limited resolution by passing the light through the lens.

Through-the-lens, laser scanning photostimulation (LSPS) allows us to widely map inputs to a single neuron at the level of a synapse (Ikrar et al., 2011, see Section 2.2). In particular, we can map pre-synaptic inputs that elicit a response at an individually recorded post-synaptic cell. Resolution at the level of a synapse is achieved by passing the laser light through the microscope's objective lens (discussed in Section 2.2). Physiologists have a finite amount of time in which to record from a post-synaptic cell while individually stimulating multiple putative inputs in order to construct a

detailed synaptic input map. In order to do this, the stimulus must be rapidly repositioned. The stimulus is rapidly repositioned among the pre-synaptic inputs using a high-speed optical scanner (see Section 1.4).

1.2 Auditory Brainstem: Circuit development and refinement of Lateral Superior Olive

The superior olivary complex (SOC, for review on circuitry see Grothe et al., 2010) of the auditory brainstem is known to be the first site of binaural integration and is involved in sound localization along the azimuthal (horizontal) plane. The head casts a shadow for higher frequency sounds which gives rise to differences in sound intensity at the two ears, referred to as an interaural level difference (ILD). The lateral superior olive (LSO), a major nucleus found in the mammalian SOC, is involved in detecting ILDs (for review see Grothe et al., 2010). Each LSO receives excitatory inputs from the ear on the same side (ipsilateral), as the cochlea sends auditory information to the anteroventral cochlear nucleus (AVCN) which relays on the information to the LSO (Moore and Caspary, 1983; Sanes et al., 1987; Glendenning et al., 1991; Bledsoe et al., 1992; Fig. 1). Each LSO also receives inhibitory inputs from the medial nucleus of the trapezoid body (MNTB), which is driven by excitatory inputs from the opposite (contralateral) ear (Moore and Caspary, 1983; Sanes et al., 1987; Glendenning et al., 1991; Bledsoe et al., 1992; Fig. 1). These converging inputs must be aligned by frequency, as ILDs are computed based on frequency (Boudreau and Tsuchitani, 1968).

Neurons spend energy and resources refining the position of their inputs. The positioning of their inputs ultimately determines the circuit's function. Refinement of input position and strength occurs in the LSO early in life and requires patterned neural activity. First, genetically determined

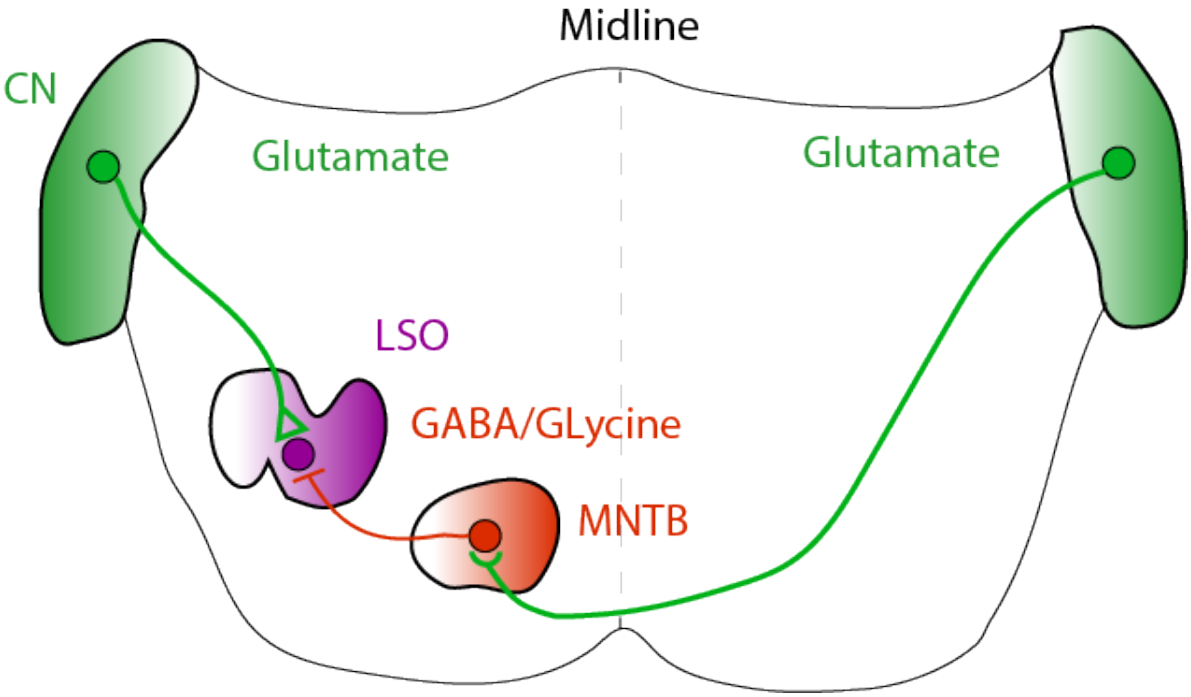

Figure 1: Schematic of coronal brainstem section, showing the synaptic organization of the anteroventral cochlear nucleus (AVCN, green), the lateral superior olive (LSO, blue) and medial nucleus of the trapezoid body (MNTB, red). Principal cells in the LSO integrate excitatory glutamatergic inputs from the ipsilateral AVCN with inhibitory inputs from the MNTB, which receives inputs from the contralateral AVCN.

cues, that are not the focus of this review, direct the axons (approximately) to the right location in the target nucleus. Subsequently, synapses are strengthened or weakened through patterned neural activity, a process that can be measured using electrophysiological approaches, and the neurons undergo morphological changes that can be measured using anatomical approaches. In this literature review, I will focus on the physiological processes of refinement and will discuss using photostimulation techniques to mimic patterned neural activity.

During the period of refinement, functional connections carrying similar sound frequency information (tonotopic) become fine-tuned together. These inputs are spatially arranged such that inputs carrying information of tones close in frequency are represented in neighbouring regions of the LSO. The refinement of these inputs occurs in both the MNTB-LSO and AVCN-LSO pathways between postnatal day 3 and 8 (P3/8) (Case et al., 2011). During this period, the current amplitude of a single input in the MNTB-LSO pathway increases 12-fold, indicating an increase in input strength. During the same period, the area of MNTB capabe of eliciting a response in a single LSO cell decreases (Kim and Kandler, 2003), indicating pruning inputs. During this same time period, the current amplitude of a single input in the AVCN-LSO pathway increases by 5-fold, and the number of inputs from the AVCN to a single LSO neuron decreases (Case et al., 2011). Hearing onset in rodents occurs by P12, suggesting this functional refinement occurs without acoustically driven activity. The refinement of the MNTB-LSO and AVCN-LSO pathway relies upon internally generated neural activity before hearing onset (Clause et al., 2014).

Sensory systems develop through activity-dependent plasticity. This activity can be generated spontaneously within a sensory organ (Galli and Maffei, 1988; Meister et al., 1991; for review see: Katz and Shatz, 1996). In the visual system, the retina generates patterned bursts of spontaneous

activity which is needed to refine the projections to the thalamus (Penn et al., 1998). Removal of the cochlea can prevent refinement in the developing auditory brainstem (Russell and Moore, 1995), suggesting an important role of spontaneous activity generated by the cochlea in the developmental circuit refinement of the auditory brainstem. Creation of spontaneous activity in the mammalian cochlea has been characterized (Tritsch et al., 2007). Adenosine Triphosphate (ATP), spontaneously released from supporting cells of the Kolliker's organ, depolarizes inner hair cells (IHC). If the IHC is depolarized sufficiently, it will generate Ca^{2+} spikes that lead to glutamate release from the IHC onto spiral ganglion neurons. Enough activity in the spiral ganglion neurons results in action potentials in the auditory nerve. The spontaneous ATP-dependent activity in the cochlea begins around P3 and tapers off at hearing onset (Tritsch and Bergles, 2010). This period of spontaneous activity, which is transmitted into the auditory brainstem, coincides with the period of refinement in the MNTB-LSO and AVCN-LSO pathways (P3-P8).

Circuit-level changes are made during the period of refinement and allow for cells to integrate information accurately. Below I will discuss how we can use through-the-lens LSPS to artificially stimulate the MNTB-LSO and AVCN-LSO pathways to study how these circuits are coordinately refined.

1.3 Laser Scanning Photostimulation in the MNTB-LSO and AVCN-LSO Pathways

The LSO is an excellent model system to study how tonotopic maps are refined. As previously mentioned, it receives excitatory inputs from the ipsilateral AVCN and inhibitory inputs from the MNTB which is driven by the contralateral AVCN. These converging inputs carry tonotopically

matched information from both ears.

During postnatal development, excitatory AVCN inputs and inhibitory MNTB inputs onto the LSO principal neuron are redistributed. To study these synaptic changes, we need to map these inputs over postnatal development and determine their strength as a function of position. This requires stimulating the AVCN and MNTB synapses (separately) on the LSO principal neuron and recording the responses elicited at the cell body using whole-cell patch clamp. By using through-the-lens photouncaging, we will be able to stimulate inputs on an LSO principal neuron at the synaptic level using caged neurotransmitters (explained in Section 2.1 & 2.2). The excitatory inputs of the AVCN release glutamate (Wu and Kelly, 1992); the inhibitory inputs of the MNTB release gamma-amino-butyric acid (GABA) in addition to glycine (Kotak et al., 1998; Korada and Schwartz, 1999; Nabekura et al., 2004). The inhibitory MNTB-LSO synapses initially release GABA until the second postnatal week, when there is a switch to predominantly glycine release. To create a detailed map of the inputs, we need a sub-micron grid of stimulation sites over our LSO principal neuron. This requires quick and efficient guidance of the light source across the cell. Below I will talk about the common methods of repositioning the light source, their benefits and limitations.

1.4 Optical Approaches in Laser Scanning Photostimulation

Fibre Optic Cable

For many situations, a single optical fibre, placed in close apposition to the tissue slice, is sufficient for focal photolysis of caged compounds. As for uncaging spot size, fibre cable diameters can be as small as $5\mu m$ (Kandler et al., 2013). The use of an optical fibre is simple, inexpensive, and can be implemented without making any modifications to an existing microscope set-up. The construction of this uncaging system requires minimal knowledge in optics, which is convenient.

Optical fibres are less desirable for high-resolution photolysis. The fibre's resolution is restricted by its core diameter, and the light emitting from the fibre diverges and thus cannot be focused to a sub-micron diameter spot on or inside the sample. The fibre cable must be placed as close as possible to the sample as the intensity of the spot decreases with distance from the fibre and reduces the probability of an uncaging event. Another major limitation of an optical fibre is that the fibre must be repositioned physically from one uncaging spot to another, increasing the possibility of mechanical disturbances or damage to the tissue. Repositioning the optical fibre is also a time-consuming process which may affect recordings because the slice's health degrades with time.

A fibre optic approach is inappropriate for this implementation as fibre cables are unable to uncage at the linear sizes required to stimulate our neurons at the level of the synapse (Helfert et al., 1992).

Digital Micromirror Device

One way to rapidly reposition a light is with a digital micromirror device (DMD). A DMD contains an array of 1024x768 (XGA) or 1920X1080 (1080p) separate mirrors. These mirrors can be switched independently from an 'ON' position to an 'OFF' position ($\pm 12°$, Fig.2). The 'ON' position directs the light towards the specimen (along the optical axis) whereas the 'OFF' position directs the light towards a beam stop (Fig. 3). Each mirror defines a pixel (point), and when in the 'ON' position, projects the light to a point on the sample. This means a DMD is able to generate random spatiotemporal light patterns by selectively choosing individual mirrors to turn on. The temporal resolution can be sub-millisecond due to the fast switching rate of the mirrors.

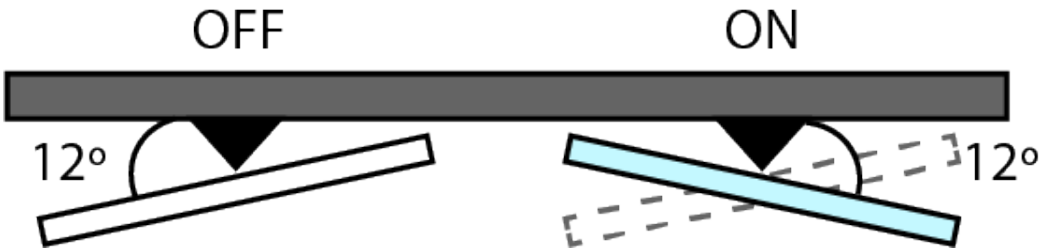

Figure 2: Schematic of the side view of a digital micromirror device (DMD) mirror. Mirrors can be switched between the 'OFF' state (white) and the 'ON' state (blue) by rotating the mirror by 24 degrees in either direction.

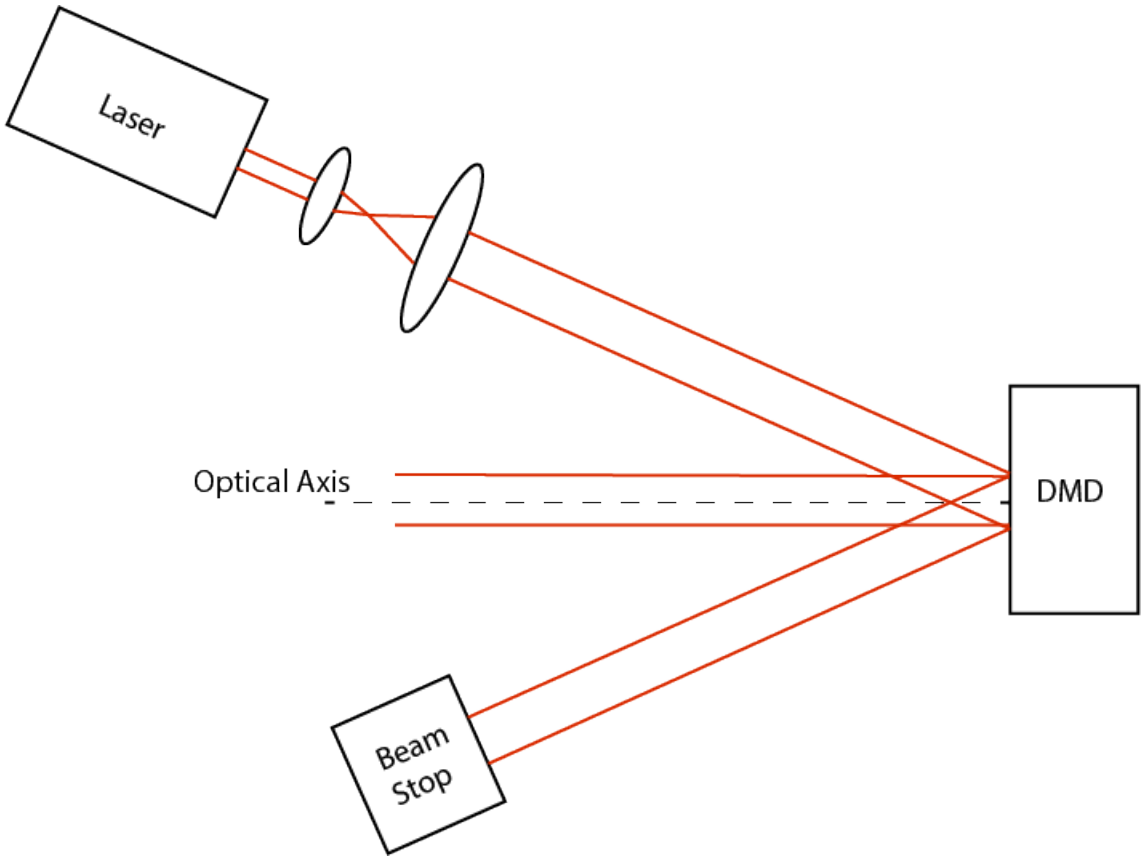

Figure 3: Schematic of a typical DMD optical pathway. When the DMD mirror(s) is in the 'ON' position, the light is directed toward the optical axis (towards the sample). When the DMD mirror(s) is in the 'OFF' position, the light is directed towards the beam dump.

Digital Micromirror Devices are a viable option for controlled photostimulation both spatially and temporally. However, they lack robustness. The mirrors are calibrated to reflect a limited bandwidth of light. This poses a problem when attempting to uncage multiple caged compounds of various excitation wavelengths (refer to Table 1). Since each mirror of the DMD directs light towards a point on the sample, the spatial resolution between uncaging points is limited by the distance between the centers of each mirror. The gaussian power distribution of laser light means the mirrors on the outer edges of the DMD reflect laser light of lower power. Therefore, a costly, high-powered laser is needed. We desire robustness in our photouncaging system which a DMD does not provide.

Acousto-optical Deflector

Acousto-optical deflectors (AODs) are a high-speed, high-spatial resolution scanning technology. AODs deflect light by taking advantage of the photoelastic effect. Photoelasticity refers to the change in optical properties of a material under mechanical stress. In the case of an AOD, the interaction of sound, radio frequency (RF), and light in a crystalline material is an example of the photoelastic effect. A RF wave is driven into the AOD's crystal core using a piezo-electric transducer. The RF wave travels from transducer to absorber and creates areas of compression and rarefraction inside the crystal. Different frequencies of RF waves cause varying patterns of compression and rarefraction thus changing the crystal's refractive index as a function of RF frequency. AODs are designed to maximize refraction to a first-order position (θ_d, Fig. 4) by aligning the angle of the incident laser beam to the Bragg angle (θ_B, Fig. 4). The Bragg angle is given by:

$$\theta_{bragg} = \frac{\lambda f_a}{2V_a} \tag{1}$$

where f_a is RF frequency, λ is wavelength of laser and V_a is acoustic velocity.

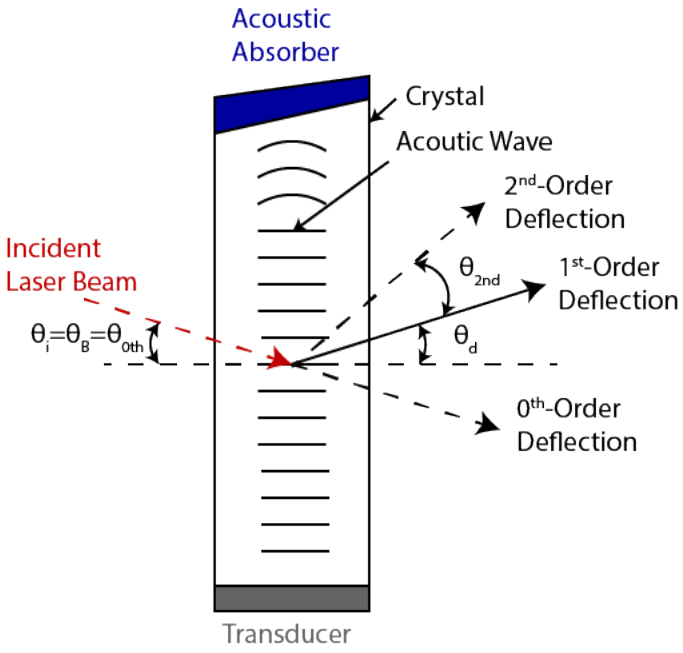

Figure 4: Schematic of the configuration of an acouto-optical device (AOD).

When aligned to the Bragg angle, the deflection angle of the laser light at the output (θ_d) is given by:

$$\theta_d = \frac{\lambda f_a}{2nV_a} \tag{2}$$

where n is the refractive index of the crystal when undisturbed. Higher order refracted light undergoes destructive interference and is not observed (θ_a, Römer and Bechtold, 2014, Fig. 4). With the incident laser angle fixed, the deflection angle at the output varies with the RF frequency. The maximum deflection angle is proportional to the RF frequency bandwidth (Δf_a) used, given by:

$$\Delta\theta_d = \frac{\lambda \Delta f_a}{2nV_a}. \tag{3}$$

Another important parameter of an AOD is the acoustic power of the RF wave. The energy effi-

ciency of the first-order refracted light is a function of the acoustic power. The higher the acoustic power, the higher the optical intensity in the first-order position (conversely, the lower the optical intensity in the zeroth-order position, Fig. 4). In principle, an AOD's laser deflection angle is controlled by adjusting the RF frequency, and the laser intensity is controlled by adjusting the RF power.

Acousto optical deflectors are a powerful tool for laser scanning, providing extremely fast switching time from one uncaging position to another (approximately $10\mu sec$). Response time of an AOD is the time taken for the acoustic wave to fill the opening that allows the light to pass through the AOD (optical aperture). This response time is given by:

$$T_a = \frac{D_{Beam}}{V_a} \tag{4}$$

where D_{Beam} is the beam diameter. This deflection velocity is constant over all scan angles; the time for a small angle step is equal to that of large angle step. This fast response time is enhanced further with the AOD's superior angular accuracy. The AOD is controlled digitally and has no weighted mechanical part that removes of any inertial forces that would normally affect angular accuracy.

As AODs constitute a relatively new scanning technology, the crystal mediums used for AODs have not yet been optimized for high intensity, first-order deflections. The AOD loses $25 - 45\%$ of the laser power at the output to higher order refracted light. For this reason, Δf_a is chosen to maintain $55 - 75\%$ of the laser intensity (measured empirically). This constraint reduces our maximum frequency bandwidth and reduces our maximum deflection angle (Eq. 3). A reduction in maximum deflection angle results in smaller scanning area which is our uncaging area. Mirror galvanometer scanners are a more established scanning technology compared to the relatively new AODs.

Mirror Galvanometer Scanner

Galvanometer-based optical scanners (galvos) are the most common solution for many scientific, imaging and laser applications. They are robust, fast and precise. A galvo system is made of three components: the galvanometer, the mirror, and the servo driver that controls the galvo. The galvo itself is made up of the actuator and the position detector. The actuator is responsible for controlling the mirror's movement, and the position detector provides mirror positioning information to the servo driver. The choice of mirror greatly affects the speed and accuracy of positioning and must be thought about carefully. At the simplest level, the mirror must have high reflectance at our specified wavelength and must contain the required beam diameter. More detailed specifications such as mirror thickness, materials and weight are all important and affect the galvo's response time and repeatability. These specifications should be provided by the manufacturer. The final component of the galvo system is the servo driver. The servo compares the current position signal of the mirror to the signal of the next command and drives the actuator to bring the galvo to the commanded position. The driver aims to bring the difference between the two signals close to zero. The galvanometer, mirror and servo driver work cooperatively for successful positioning of the galvo system.

Random-access imaging refers to the illumination of spots at any location on our sample rather than following a fixed sequence, and random-access photouncaging requires step-and-hold position from the galvo. The system is driven to a fixed angle and is held there as the procedure is performed. This positioning requires highly precise and repeatable beam placement, which are important design criteria to consider when choosing a galvo (Refer to section 3.2 for calculations). The mirror size ultimately affects positioning precision and velocity, with the largest of mirrors (20mm) having a small angle step response of approximately $600\mu sec$ (Canon USA Inc., San Jose). However, this

step response increases with larger angular movements. Galvos from Canon USA were chosen as it met our specifications, budget, and there was local expertise working with this scanhead. The speed and precision of galvos allow us to uncage hundreds of thousands of spots, precisely and relatively fast.

When compared to an AOD, the galvo lacks in scanning speed and angular resolution. As mentioned before, an AOD's constant deflection speed over any angle makes its large angle step response superior to that of a galvo. Driving the galvo for faster positioning would only increase dynamic errors. The angular resolution of the galvo is inferior to an AOD due to the inertial forces caused by the galvo's weighted components. Aside from these limitations, we still believe the galvo is the most appropriate for this implementation.

Galvo mirror designs have been optimized, providing high reflectance at many desired wavelengths. This is important when dealing with more dangerous lasers where high throughput at the galvo mirrors means low energy needs at the source. Wider scan angles from the galvo allow us to map a larger area of our neuronal circuit with more resolvable uncaging spots. Galvo's are relatively inexpensive and are very robust. They provide us the temporal and spatial resolution needed for our synaptic-circuit mapping while giving us the opportunity to build and explore new options.

2 Through-the-lens Photouncaging

2.1 Photouncaging

Caged Compounds

Photouncaging uses light to interact with light-sensitive caged compounds. Caged compounds are biological molecules that are biologically inactive by addition of a photolyzable "caging" molecule (for review see Adams and Tsien, 1993). When provided the appropriate energy light (determined by the number and wavelength of photons), the "caging" molecule absorbs energy (in the form of a photon) and undergoes a conformational change. This event leads to a separation of the caging molecule from the rest of the molecule. The molecule may then go on to interact with its nearby biological target (Fig. 5). With the right equipment, photouncaging can be done with high temporal and spatial resolution.

For our experimentation, we will use caged neurotransmitters. More specifically, we will be using caged glutamate, caged GABA and caged glycine (refer to Table 1). To evaluate our caged neurotransmitters, we inspect three important properties. These caged neurotransmitters should have minimal interaction with our biological system of interest, more specifically, to the receptor of interest. Second, the by-products of the photolysis should not interfere with the natural processes of the uncaged molecule or its relevent systems. It is difficult to test caged compounds for agonist and antagonist activity at every presumed target (for review see Sarkisov and Wang, 2007), we must design our photouncaging experiments with this in mind. Lastly, the caged neurotransmitter must be photolyzed quickly and efficiently in response to illumination. We consider a parameter known as the uncaging index (UI), defined as

$$UI = \epsilon\varphi \tag{5}$$

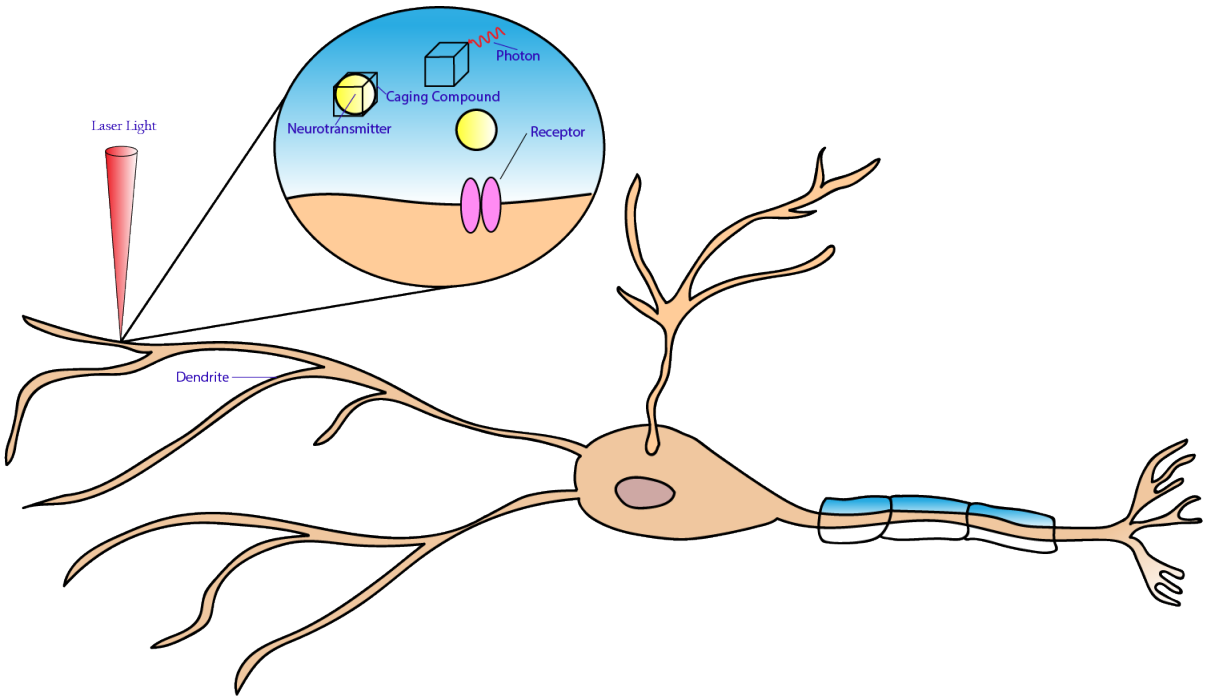

Figure 5: Schematic representation of synaptic activation via photouncaging. The desired neurotransmitter is made inactive by addition of a caging molecule. When a sufficient amount of energy is absorbed (in the form of a photon), the caging molecule separates from the neurotransmitter. The neurotransmitter may then go on to interact with its target receptor.

Cage	$\lambda_{excitation}$ (nm)	Reference
Glutamate		
MNI-caged glutamate	350	(Momotake et al., 2006)
CNB-caged glutamate	350	(Momotake et al., 2006)
BNSF-Glu	415	(Ellis-Davies, 2011)
CDNI-Glu	720	(Ellis-Davies, 2007; Kantevari et al., 2010)
MNI-Glu	730	(Matsuzaki et al., 2001) (Ellis-Davies, 2007)
RuBi-Glu	800	(Fino et al., 2009)
GABA		
RuBi-GABA	473	(Rial Verde, 2008)
CDNI-GABA	720	(Richers et al., 2017)
N-DCAC-GABA	720	(Kantevari et al., 2010)
G5-DEAC450-GABA	900	(Richers et al., 2017)
Glycine		
DECM-caged glycine	350-450	(Shembekar et al., 2007)
NI-caged glycine	350	(Ueno et al., 1995)
C2-caged glycine	350	(Ueno et al., 1995)

Table 1: Various caged compounds for glutamate, GABA and glycine with their respective excitation wavelengths. Compounds presented are for one and two-photon uncaging.

where ϵ is the extinction coefficient and φ is the quantum yield. Quantum yield is the probability of a caging molecule to be photolyzed after absorbing energy from a photon. The extinction coefficient is a constant that refers to how strongly a caging molecule absorbs light at a given wavelength, per molar concentration. When light is considered a stream of particles instead of an electromagnetic wave, absorption is a molecular reaction caused by the collision of particles (Ellis-Davies, 2007). The larger the ϵ, the higher the probability that a photon will be absorbed. Hence, the UI is how efficiently the caging molecule absorbs a photon, and how efficiently the caging molecule is photolyzed once the photon is absorbed. Less light exposure is needed for photolysis of high UI caged compounds. This is an important consideration when dealing with more dangerous laser light sources, such as ultra violet (UV).

2.2 Through-the-lens Uncaging

Uncaging that uses a light source passing through the objective lens is referred to as through-the-lens photouncaging. The light source is one of the most important components of an uncaging system. It must provide enough energy at the appropriate wavelength(s) for sufficient photolysis. Xenon, flash and mercury arc lamps have been used for many photouncaging systems. However, these sources are not collimated and have significant energy losses (for review see Sarkisov and Wang, 2007). Laser light sources, which deliver high-intensity, collimated (parallel) light, are used most commonly. Advancements in laser light technology have provided us two main methods of excitation based on the chosen wavelength: one-photon and two-photon excitation (Section 2.3).

Light from the laser source arrives at the sample in discrete units called "photons." Photons have no mass, but have energy

$$\begin{aligned} E &= hf \\ &= \frac{hc}{\lambda} \end{aligned} \tag{6}$$

where $h = 6.626x10^{-34}Js$ is the universal Planck's constant, c is the speed of light, and λ is the wavelength of the light. The energy of a photon is inversely proportional to the wavelength of the light. Photons of shorter wavelength light have more energy than photons of longer wavelength light. When a photon interacts with a molecule, an energy transfer may occur between the photon and an electron of the molecule. The photon either deposits all of its energy onto the electron, or none at all. This is the mechanism behind photoexcitation.

The caged compound when first applied to our sample is in a low-energy state called the ground state. When excited to a high-energy state, the caging molecule undergoes a conformational change that causes its cleavage from the caged biological molecule. The biological molecule is then free to act upon its intended target (Fig. 5). The caged compound needs to absorb a sufficient amount of energy, fast enough to change from its ground state to its high-energy, excited state (Fig. 6). The energy absorbed is from photons delivered by our laser source. Before arriving at the sample, the laser light is passed through various optical components and finally the microscope's objective lens. By taking advantage of the properties of an objective's converging lens, we can excite our caged neurotransmitters at the resolution imposed by our objective lens.

Ray Tracing

Parallel rays entering a converging lens along the optical axis focus to a single spot, the focal point (Fig. 7). Parallel rays entering the lens on an angle to the optical axis converge to a point on the focal plane but at an offset; the offset being determined by the properties of the lens (Fig. 8). The focal point resides on a plane called the focal plane that is a distance f (focal length) from the lens (Fig. 7). The focal length f is described by the Lensmaker equation:

$$\frac{1}{f} = (n-1)\left(\frac{1}{R_1} - \frac{1}{R_2}\right) \tag{7}$$

where n is the refractive index of the lens, and R_1 is the radius of curvature of the outer surface of the lens and R_2 is the radius of curvature of the inner surface of the lens. The Lensmaker equation makes two assumptions. First, the distance between the two surfaces of the lens is negligible, such that we do not need to account for the light travelling between the two surfaces of the lens. Second, the two surfaces can be described with a spherical radius of curvature. This equation allows us to determine how far from the lens our parallel rays will converge. Light collected by a lens from the focal plane exit the lens as parallel rays (Fig. 7). Rays emitted from a focal point at an offset from the optical axis will exit the lens as parallel rays but at an angle. This allows us to focus light with the same lens that is used to collect light (and vice versa).

As mentioned above, laser light delivers high-intensity, parallel light. This collimated light passing through our objective lens converges to a spot on its focal plane (Fig. 8). This focal point is not infinitely small; it is a distribution of intensities called an "Airy disk." The diameter of this Airy disk defines the resolution of the optical system. The resolution is defined by the equation:

$$resolution = \frac{0.61\lambda}{NA} \tag{8}$$

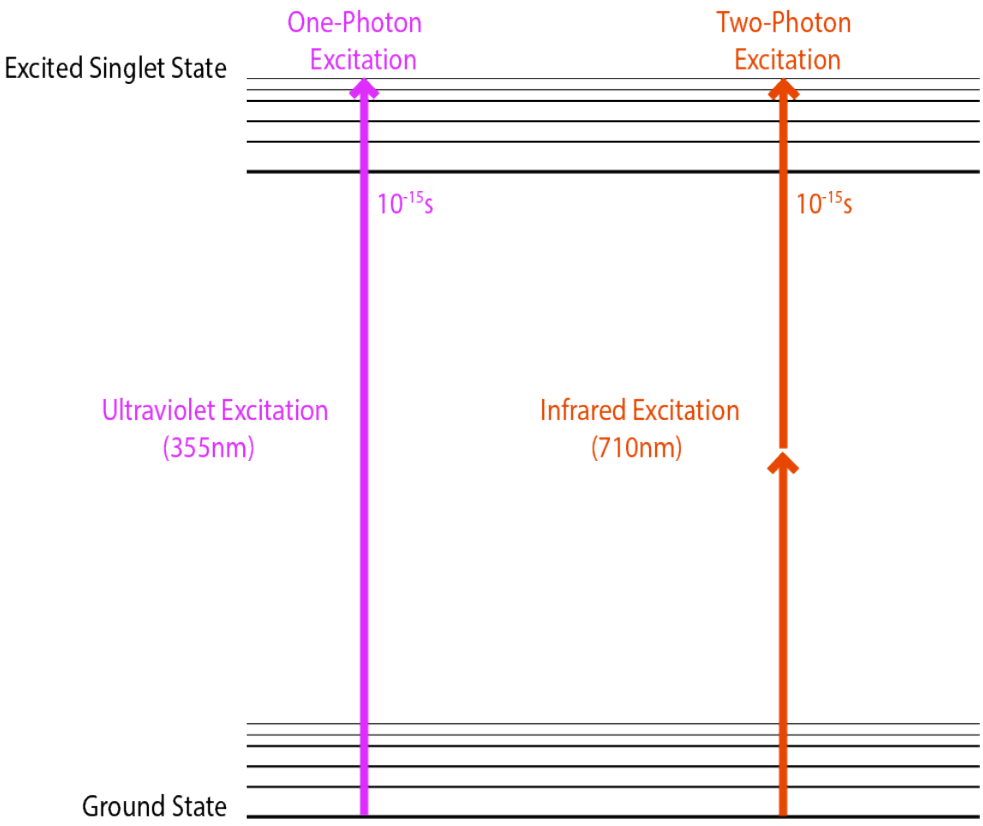

Figure 6: Jablonski Energy Diagram depicting the differences between one-photon (purple) and two-photon (red) excitation. One-photon excitation requires the energy of a single high energy, short wavelength photon to excite the molecule from ground to excited state. Two-photon excitation requires the energy of two lower energy, longer wavelength photons to excite the molecule from ground to excited state. The wavelength of the two-photon excitation is about twice that of one-photon excitation.

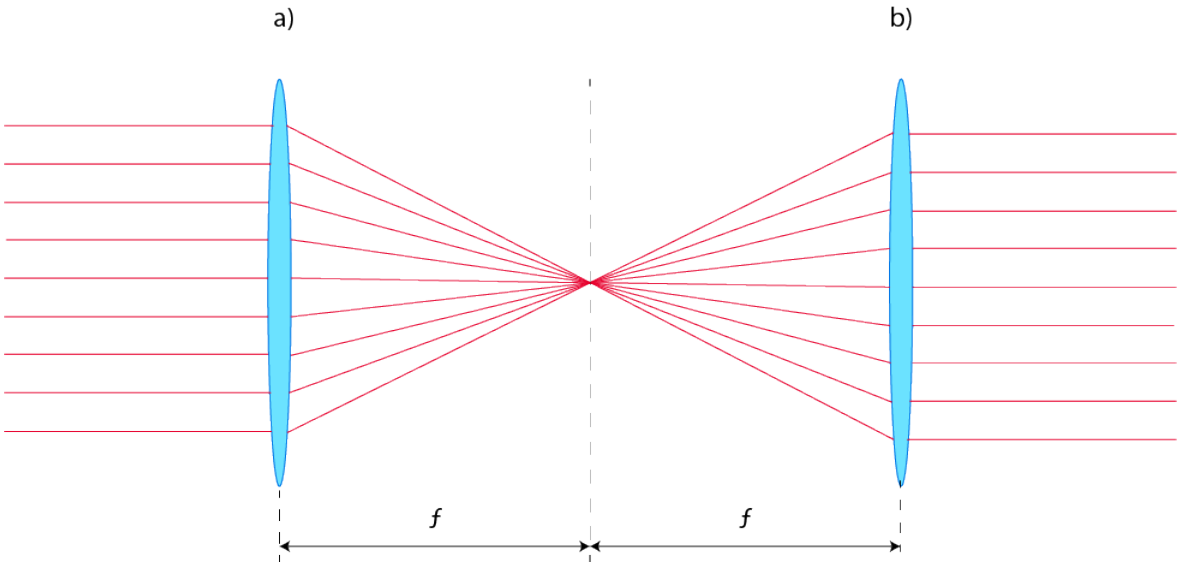

Figure 7: a) Parallel rays (to the optical axis) entering a converging lens focus to a single spot called the focal point. This focal point resides on a plane called the focal plane which is a distance f from the lens. f is determined by the properties of the lens. b) Light collected by a lens from the focal plane exit the lens as parallel rays.

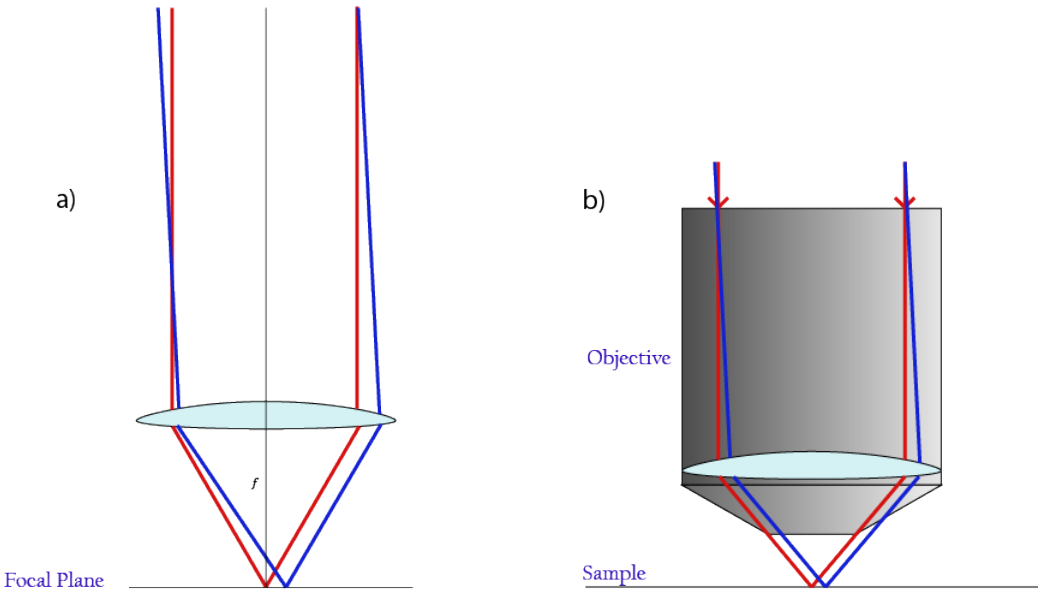

Figure 8: a) Parallel rays (blue) entering a lens at an angle converge on the focal plane at an offset to the optical axis. Parallel rays (red) entering along the optical axis converge on the center of the focal plane. b) At the objective lens, this property is used to scan the focal spot across our sample.

where λ is the wavelength, and NA is the numerical aperture of the lens. By carefully selecting the wavelength of light, and the numerical aperture of the objective lens, we can control the resolution of our system and the size of our excitation spot. The highest numerical aperture objective lenses can achieve resolution of $200 - 550nm$ at most wavelengths. Relative to the size of a synapse on an LSO principal cell -$0.5 - 1\mu m$- this resolution should allow us to excite a bolus of neurotransmitters sufficient to stimulate an individual synapse (Helfert et al., 1992).

2.3 One-photon and Two-photon Excitation

The wavelength of the light affects both the energy of the photons (Eq. 6) and the resolution of our system (Eq. 8). There is no correct wavelength in photouncaging but the two primary excitation methods for photostimulation, one-photon and two-photon excitation, work best in certain wavelength ranges. Both photouncaging methods have their advantages and disadvantages with respect to cell health and quality of uncaging.

One-photon Excitation

As the name suggests, one-photon excitation requires the energy of a single photon to bring the caged molecule to its excited state. Absorption of light occurs rapidly (on the order of femtoseconds, 10^{-15}, Fig. 6) in discrete packets and can result in the excitation of the caging molecule (Fig. 6). Relaxation of the excited state to the ground state is slower (on the order of picoseconds, 10^{-12}, Fig. 6). The caged molecule must absorb the energy needed to reach its excited state from one absorption event or it will remain in its ground state. For this reason, a single photon of high energy is the simplest method to excite our caged compound. Shorter wavelength light is used in one-photon excitation because it contains higher energy photons. Most commonly, UV ($355nm$) or near-UV wavelength light is used for one-photon excitation. For my thesis, I will focus on using UV

light ($355nm$) in one-photon excitation.

One-photon excitation has one powerful advantage over two-photon excitation. The shorter wavelength light provides higher resolution uncaging spots (Eq. 8). Using a shorter wavelength light, however, has many disadvantages. First, the highly energetic photons of UV light are phototoxic to living cells. The health of our living slice is highly sensitive to UV light exposure, and we must be cautious of this during experimentation. To maximize cell life, UV laser power at the sample is limited to $15mW$, which is sufficient to uncage our caged neurotransmitters (Shepherd and Svoboda, 2005). The power of our laser can be controlled by using neutral density filters (NDFs), which reduce the intensity of light passing through them. Second, shorter wavelength light has shallow depth penetration within our sample. The scattering of the photons is proportional to $\frac{1}{\lambda^4}$, where wavelengths in the UV range could have 25 times the scattering of wavelengths in the near-infrared (NIR) range. Scattering photons affect the amount of caged neurotransmitters that are uncaged and the spatial area over which it is (Fig. 9). Finally, UV laser light poses an increased risk to lab personnel. The laser must always be operated with the appropriate personal protective equipment, and the appropriate measures must be taken to protect the surrounding equipment (UV graded optics, blackout curtains and boards).

Two-photon Excitation

Two photon excitation (also known as multiphoton excitation) is considered the best option when interacting with living cells. Compared to one-photon excitation, multiphoton excitation is relatively harmless to living cells as it relies on lower energy photons. Two-photon excitation occurs after a target molecule absorbs energy from two photons in an extremely short period of time (near-simultaneously). Each of the two photons carries approximately half the energy required to excite the molecule. Since the energy of a photon is inversely proportional to its wavelength (Eq. 6), the wavelength of the two photons absorbed is usually about twice that required for one-photon excitation. As shown in Figure. 6, a caged compound that is normally excited by a single $355nm$ wavelength photon can be excited by two $710nm$ wavelength photons if both arrive at the caged compound in approximately the same time (within 10^-18 seconds of each other). This requires a high-power, femtosecond laser; a laser in which the power at the peak of the pulse is high enough for significant two-photon excitation, while the average laser power remains low. The resulting excited state of the caged compound from two-photon excitation is the same that follows one-photon excitation (Fig. 6).

Two-photon absorption events are rare, and in order to produce a significant number of events the photon density must be one million times that required for one-photon absorption (Benninger and Piston, 2013). We can increase the probability of two-photon absorption events by focusing the laser light through the microscope's objective (through-the-lens). As the laser beam comes to a focus, the photons become more tightly packed, increasing their spatial density, thus increasing their chances of interacting. Additionally, the focal point is the only location along the cone of excitation where the photons are dense enough to cause significant two-photon absorption events (Fig. 9). Above and below the focal point, the photons are not dense enough for significant numbers of

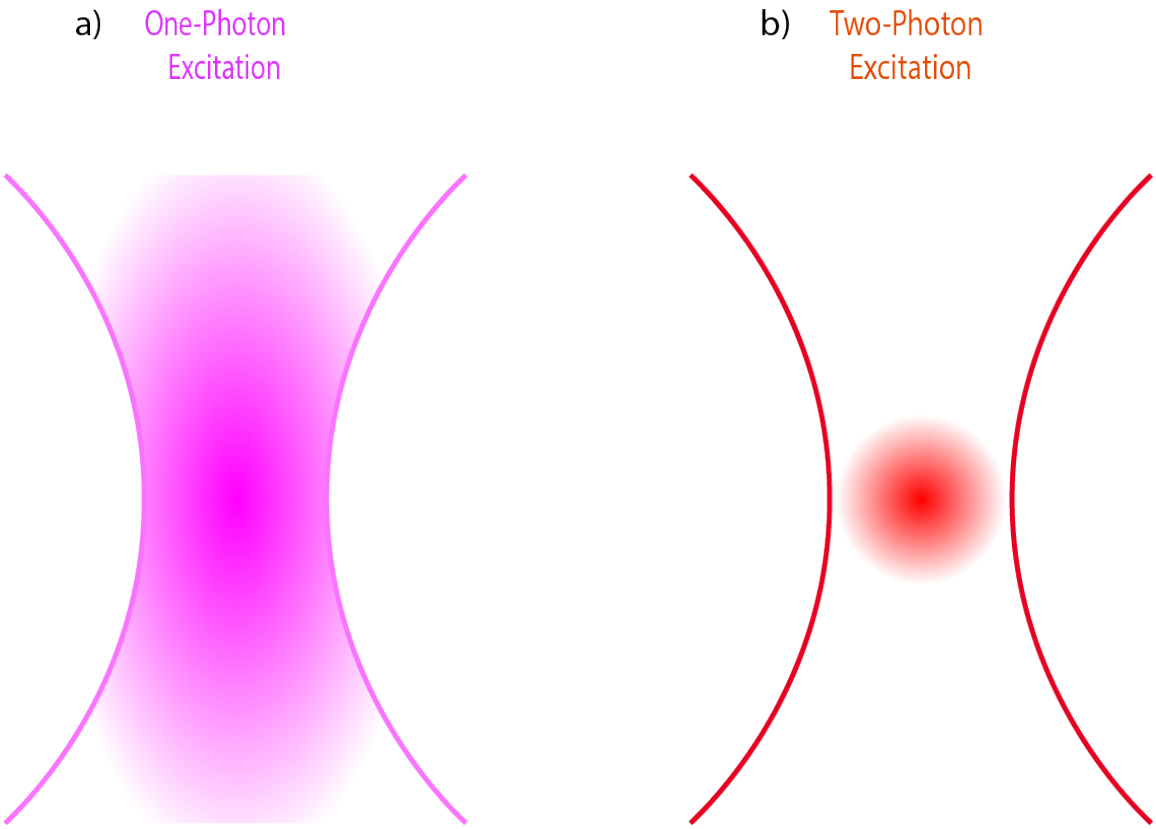

Figure 9: a) Once focused, one-photon absorption occurs throughout the cone of excitation as it depends linearly on excitation intensity. One-photon absorption is diffused further from scattering of shorter wavelength photons. b) Once focused, two-photon absorption occurs only at the focal plane as the probability of a two-photon event is highest at the focal plane.

absorption events to occur. This property of two photon uncaging allows us to precisely uncage our caged neurotransmitters. Scattering of photons is also heavily reduced at longer wavelengths, allowing for deeper tissue penetration. One drawback is a loss of resolution (Eq. 8). NIR wavelengths can achieve uncaging spots of $0.5\mu m$ in diameter, a size sufficiently small to stimulate individual synapses in our system (Helfert et al., 1992).

Two-photon excitation has many advantages over its one-photon counter-part. First, two-photon excitation has higher axial resolution. Second, the absence of two-photon absorption from

out-of-focus laser light allows for deeper and more spatially precise uncaging. This provides deeper and more precise uncaging events. Finally, two-photon excitation minimizes photodamage to our living tissue. Much is still unknown about the mechanisms underlying light-induced cell damage and, practical experience shows that NIR excitation does not affect cell health. Cell health may be unaffected because two-photon absorption is confined to the focal plane (Benninger and Piston, 2013).

Summary

The LSO is a great model system area where inputs of opposing signs are coordinately refined. How this coordinate refinement occurs is an important question not yet answered. We aim to study the distribution and redistribution of these inputs during development using through-the-lens photouncaging. Because two-photon excitation is more appropriate than one-photon excitation for our uncaging experiments in living tissue, a two-photon system is the ultimate goal. The purpose of the present project is to demonstrate feasibility using an available UV laser, in order to apply for funds to acquire the femtosecond laser required to convert this system to a two-photon uncaging system. Below I will describe a custom-built, through-the-lens UV uncaging system to map synaptic inputs.

3 Design

3.1 Design Overview

I began designing the optical system by identifying the primary goal. This goal is to guide the laser light from source (UV laser), into the microscope, and finally onto the sample. The next step is to determine the modifications needed to be made to the laser light between the source and sample. These modifications to the light include laser power control, beam redirection, and beam expansion. My research and findings finalized the optical design, and the parts needed to be purchased (Fig. 10). Over the course of my studies, I have extensively researched dozens of different photouncaging designs. I researched and compared different scanning technologies (see Section 1.4), excitation methods (see Section 2.3), and optical parts that are optimized for both UV and NIR. Below, I will describe in depth our optical design including the parts required and how they meet the specifications of our design question.

3.2 Key Parts

UV Laser

The light source is arguably the most important component of an optical system. It is the deciding factor when considering which parts to purchase and influences the caged compounds we use. The light source is important for future-proofing the system for other imaging techniques such as calcium-imaging, voltage-sensitive dyes and more (outside the scope of my thesis). This implementation uses a UV laser as the light source. This decision was made for reasons of the expediency, due to the existence of an appropriate UV laser and the projected cost of the preferred femtosecond laser ($\approx \$200K$ CND). Our designs will help a future lab member implement a two-photon uncaging system. For my thesis, I will be focusing on our UV photouncaging design, and I will discuss our

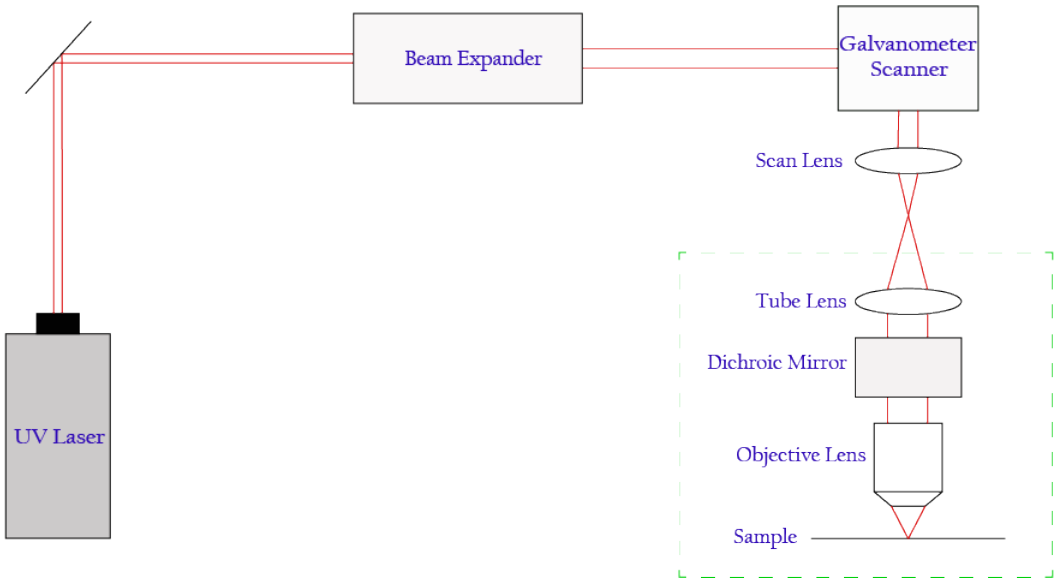

Figure 10: Optical path of the ultraviolet (UV) through-the-lens photouncaging system. The laser light is redirected from laser source (DPSS Series 3500 UV Laser, Santa Clara) towards the beam expander (Lenstek BX-Z-355-2-8X, China). The beam is expanded and continues towards the mirror galvanometer (Canon U.S.A. GM-1010 Digital Encoder Galvano Scanner, San Jose). Two UV graded, dielectric mirrors (Thorlabs BB05 Dielectric Mirror, New Jersey, not shown) are used to guide the light vertically to the top-back port of the Olympus BX51 microscope where a scan lens (Lenstek FL-355-112-160, China) is placed. The light travels towards the scan lens, through the microscope's tube lens, and then reflects perpendicularly towards the objective (Olympus LUMPLFLN 40XW) and sample using a UV grade dichroic mirror (Chroma Technology 380dcip, Vermont) placed inside the microscope.

two-photon system in Section 4.

We are using a $100mW$ UV laser with a $1.5mm$ diameter laser beam (DPSS Series 3500 UV Laser, Santa Clara). This is considered a high-powered laser and safety precautions must be enforced. UV laser safety glasses (Thorlabs LG10 Laser Safety Glasses, New Jersey) must be worn by laser operator and other personnel within eyeshot of the laser. Laser safety glasses are graded with an optical density (OD), which is the order by which the saftey glasses attenuate light passing through it. The LG10 laser safety glasses have an OD of 7 (attenuates the laser light by 10^7) in the UV and NIR wavelengths. The table holding the optical system is surrounded by black-out boards (Thorlabs TB4 Black Hardboard, New Jersey), and the work area is covered by black-out curtains. UV light is also detrimental to skin, and any exposed skin is covered when laser is in operation. All users should complete eye exams before operating the laser, and should undergo regular check-ups during the course of use. Unfortunately, the UV laser poses as much a danger to the operator as it does the tissue being studied.

The 100mW, UV laser can be highly damaging to the tissue slice. In order to maintain cell health, we must reduce the laser power to the minimum amount of power needed for uncaging which is $15mW$ (Shepherd and Svoboda, 2005). To bring the power level down to $15mW$, we use NDFs. NDFs are graded with an optical density, and we use a series of NDFs of different ODs to bring down the laser power.

$$Power_{out} = \frac{Power_{in}}{10^{OD_1+OD_2+...+OD_n}} \tag{9}$$

Equation 9, describes the power attenuation of a laser light passing through a series of NDFs where OD_1, OD_2 etc., are the ODs of each NDF in the series. We are using a broad spectrum NDF (Thorlabs NDUV Fused Silica Reflective NDFs, New Jersey) covering $200 - 1200nm$ wavelengths.

This allows us to use these NDFs with UV wavelengths as well as NIR. To streamline the power attenuation, a fixed NDF is attached directly onto the laser aperture, and a removable or interchangeable NDF(s) is placed along the optical path for further laser power attenuation. This allows us to manually control the power output of the laser quickly (Eq. 9). However, when determining the power supplied at the sample, we must consider the power loss we see from the optics in between (scanner and objective lens). We are not concerned with losses at the UV and dichroic mirrors as they are highly efficient UV graded mirrors (above 99% reflectivity, Thorlabs BB05 Dielectric Mirror, New Jersey), and the beam expander has high transmission in the UV. The dichroic mirror (Chroma Technology 380dcip, Vermont, Fig. 11) is a specialized mirror with significantly different reflection (and transmission) properties at two or more different wavelengths, and it is placed inside the Olympus' filter turret. The dichroic mirror redirects the UV laser light entering the back of the microscope perpendicularly towards the objective lens and sample. It transmits wavelengths over $400nm$ for imaging purposes. This dichroic mirror allows us to stimulate the sample using UV light while maintaining the ability to image the cell using fluorescent dyes and indicators. UV mirrors are used to contain the beam within the perimeter of the table and direct the beam to other optical components including the microscope. More importantly, they direct the beam to the galvo.

Galvanometer Scanner

My studies began with determining the appropriate scanning method for our research question. I compared the various scanning methods described in Section 1.4 on parameters such as scanning area, angular resolution and repeatability (positioning error). We decided the quick and precise mirror galvo system was the best option for our optical design. These galvos are also low maintenance and cost. We purchased the galvo system from Canon U.S.A. (Canon U.S.A. GM-1010 Digital Encoder Galvano Scanner, San Jose). The canon galvo is one of the fastest galvo on the

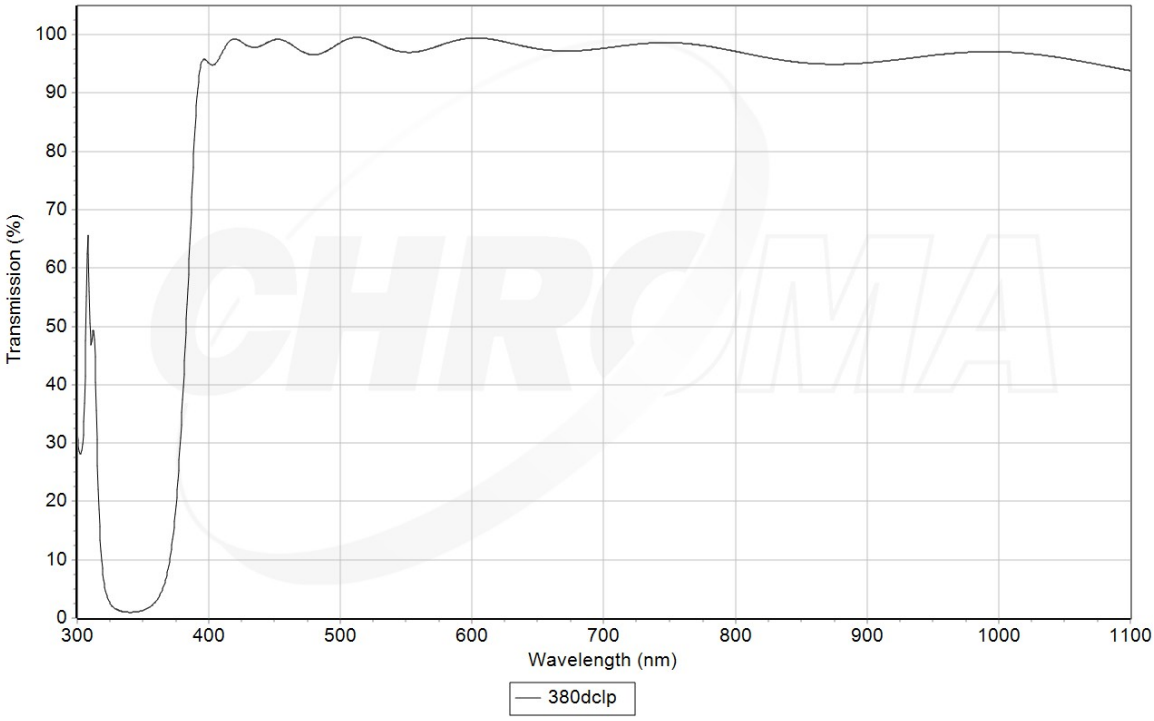

Figure 11: Figure is reproduced from the manufacturer. Transmission spectrum of the Chroma Technology 380dcip dichroic mirror (Vermont). This mirror has 99% reflectivity at $355nm$ and over 95% transmission at wavelengths greater than $400nm$. This dichroic was designed to reflect ultraviolet (UV) laser light towards our objective, and sample. It was also designed to transmit wavelengths over $400nm$ for imaging in the visible and infrared spectrum using dyes and fluorophores.

market providing high angular resolution and accuracy.

The Canon Scanner System consists of two galvo scanners, a dual axis mounting block, the motor driver unit and the system control board. Each galvo scanner has a $10mm$ diameter, silver coated mirror with 98% reflectivity in the IR wavelengths and 60% reflectivity in the UV wavelengths. Our ultimate goal is to have a two-photon uncaging system, and we chose our system with this in mind. Our galvos have significant UV intensity loses at the mirrors as the mirrors are graded for NIR. Fortunately, we still have sufficient power at the sample to uncage our neurotransmitters. These galvos are housed perpendicularly in the mount block to cover both the x and y-axis, and the motor driver unit is used to drive the galvo mirrors.

The Canon scanner is digitally controlled using a high-precision, optical encoder on the scanner and a fast, digital signal processor on the motor driver (Canon U.S.A. GC-211 Digital Galvano Driver, San Jose). The motor is driven to a certain angle determined by the number of pulses sent by the encoder. The Canon GC-211 encodes $22,756$ pulses to a 1° mechanical angle change, giving an angular resolution of $0.77\mu rad$ per pulse. This is accompanied by a position repeatability of $3\mu rad$. This parameter is defined by ISO 9283:1998 norm as the "closeness of agreement between the attained [position] after n repeat visits to the same command pose in the same direction." This can be considered the error in the galvos positioning and is a value given by the manufacturer and not empirically measured by us.

The system control board (Canon U.S.A. GB-501 Scanner System Control Board, San Jose) controls the motor driver and laser unit. It can sequentially control the scanner to redirect our laser light to any position within our scanning field (see Section 3.3). The GB-501 communicates with

the motor driver, controlling it with instructions taken from PC commands. Commands taken by the GB-501 are classified as "control commands," and "list commands." These are prioritization classifiers where control commands are processed immediately upon reading, and list commands are processed sequentially after being stored in the GB-501 internal memory. For list commands, the full list of instructions is read and stored in memory before execution.

The galvos are responsible for redirecting our laser light to any desired position within its scan angle. It is the role of the scan lens to translate the change in angle of the beam (in each axis) to a lateral shift of a focal point across the plane of focus.

Scanlens

The scan lens is put in place to translate a change in beam angle at the galvo to a change in lateral position of a focal point (Fig. 12). Without the scan lens, we do not take advantage of the resolution of our objective lens, and we see the original, collimated laser light at our sample. As mentioned in Section 2.2, a collimated beam entering a lens at an angle comes into focus at an offset from the center of its focal plane (Fig. 8). F-theta lenses, also known as scanning lenses, are corrected such that this offset has a linear relationship with the entrance angle of the collimated beam. A collimated beam entering the f-theta scan lens at an angle (θ) is focused to a point on the focal plane at a distance (Δd) of $f \cdot \theta$ from the center, where f is the focal length of the scan lens.

$$\Delta d_{scanlens} = f \cdot \theta \tag{10}$$

Most importantly, these change in position at the scan lens' focal plane (conjugate plane) are imaged

onto the sample through the optics of the microscope (Fig. 12).

$$\Delta d_{objective} = \frac{\Delta d_{scanlens}}{Magnification} \tag{11}$$

3.3 Calculations

System Specifications

This system is designed to be used with the Olympus 40X, 0.8 NA (LUMPLFLN 40XW) water immersion objective lens. The working distance ($3.3mm$) is sufficient to fit a recording electrode between the sample and objective, and the field of view ($663\mu m$) is sufficient to visualize the dendritic field of an LSO principal cell. It has a transmissivity of approximately 60% in the $355nm$ wavelength. The f-theta scan lens (Lenstek FL-355-112-160, China) is graded for high-powered, $355nm$ laser light and has an effective focal length of $160mm$. It can focus a maximum beam diameter of $8mm$ to a minimum spot size of $12\mu m$, within a scanning range of $\pm 29°$. The Canon GM-1010 galvo scanner accepts a maximum beam diameter of $10mm$ and has a scanning range of $\pm 20°$. It has an angular resolution of $0.77\mu rad$ and a repeatability of $3\mu rads$. Finally, it has a reflectivity of approximately 60% in the $355nm$ wavelength.

Scan Lens Requirements

Our scanning and objective lens have their respective focal planes in conjugate to one another (Fig. 12). For this reason, we must ensure the specifications of our scan lens are compatible with those of our objective. The calculated maximum obtainable resolution of our objective (Eq. 8) sets the limit of resolution of our uncaging spots. For illumination with $355nm$ light, this resolution is

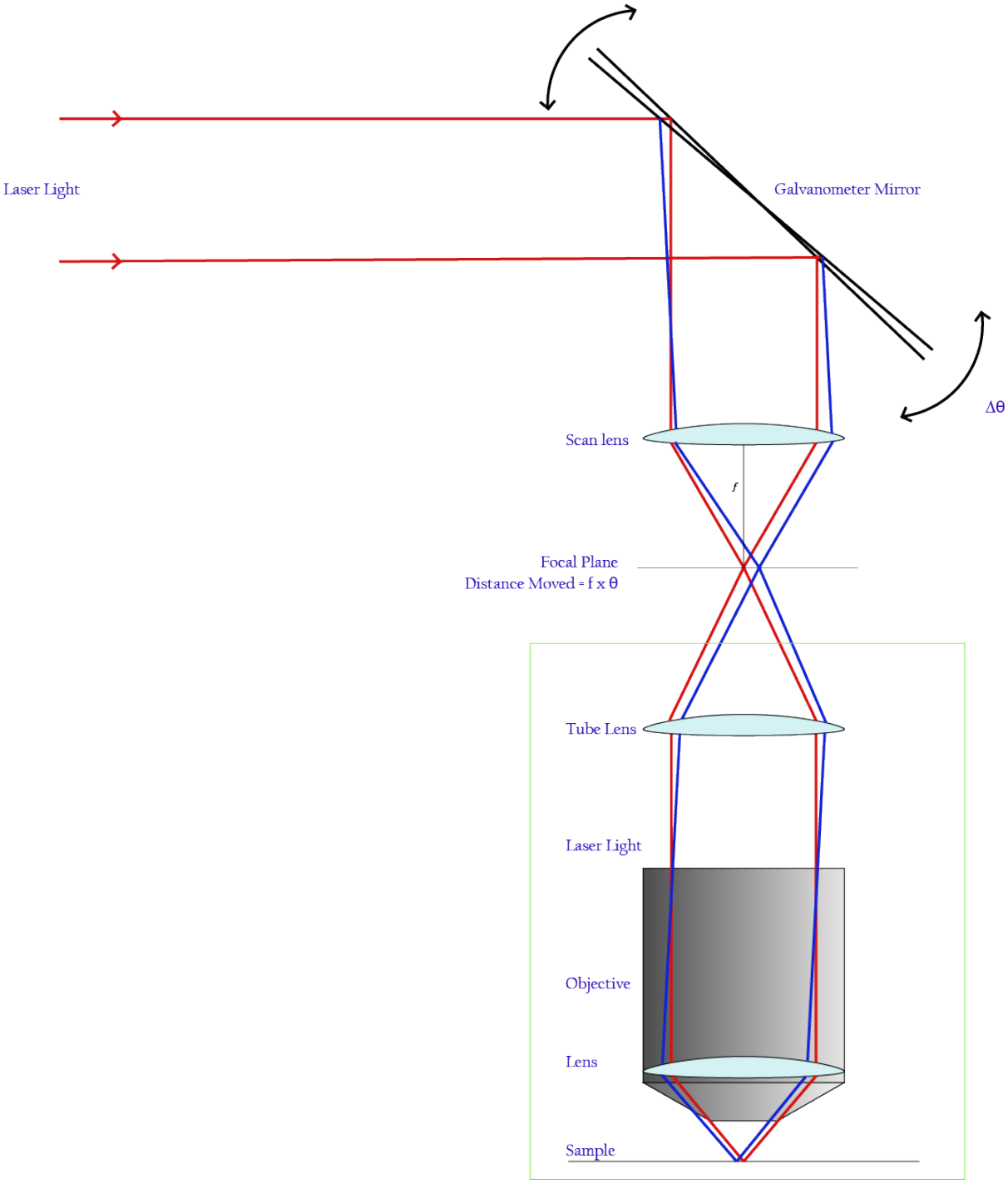

Figure 12: Schematic of an angular beam change at the mirror galvanometers being imaged onto the sample. The scan lens translates a change in laser beam entrance to a shift in focal point position on its focal plane angle (red lines indicate laser beam parallel to optical axis, and blue lines indicated beam entering scan lens at an angle). This focal plane shift is imaged by the tube and objective lens onto the sample.

$271nm$. To achieve this resolution at our sample, we need to know the resolution required at the focal plane of the scan lens (conjugate plane). Changes on this conjugate plane are ultimately imaged onto our sample (Fig. 12). Using Equation 12, we find the resolution at the conjugate plane needed to obtain a resolution of $271nm$ at the sample is $10.8\mu m$.

$$res_{conj} = res_{obj} \cdot magnification \tag{12}$$

The Lenstek scan lens can focus light to a minimum spot size of $12\mu m$ giving us a maximum resolution of $300nm$ at the sample (Eq. 12). Fortunately, this is as small as or smaller than the typical synapse onto an adult LSO neuron (Helfert et al., 1992). To focus our beam to a spot size of $12\mu m$ at the scan lens, we need to control the diameter of the laser beam entering the scan lens. This change in diameter is related to the numerical aperture of the scan lens and is described in Equation 13: where D is the diameter of the beam, f is the focal length of the lens, and NA is the numerical aperture of the lens.

$$D_{beam} \approx 2f \cdot NA \tag{13}$$

The numerical aperture at the scan lens needed to acquire a spot size of $12\mu m$ is 0.018 (Eq. 8), and the beam diameter required for this numerical aperture is $5.8mm$ (Eq. 13). This beam diameter fits within the acceptable range of our scan lens and galvo. Conveniently, resolution increases with beam diameter (Eq. 14), and any beam diameter greater than $5.8mm$ will focus to a spot size of $12\mu m$ at the scan lens. A UV beam expander (Lenstek BX-Z-355-2-8X, China) is used to magnify our $1.5mm$ diameter laser beam to approximately $6mm$.

$$res \approx \frac{1.22\lambda \cdot f}{D_{beam}} \tag{14}$$

Galvanometer Requirements

Scan lenses are used to translate a change in laser beam propagation angle to a change in lateral focal point position on its focal plane. Because of this, the performance of our galvos is greatly affected by the scan lens. We must then calculate what the angular limits of our galvo translate to in lateral positioning on our sample. First, the maximum allowable scan angle of our scan lens ($\pm 29°$) encompasses the maximum scan angle of the Canon galvo ($\pm 20°$). The galvo's angular range gives us a $1.4mm \times 1.4mm$ lateral scanning area at the sample (Eq. 10 & 11). This scanning area is sufficient to cover our objective's field of view (FOV). The angular resolution of the Canon galvo is $0.77\mu rad$, which translates to a lateral resolution of $3.1nm$ at the sample (Eq. 10 & 11). Based on ultrastructural data in adult guinea pig LSO, we calculate the distance between centers of neighboring synapses to be $0.5\mu m$ (Helfert et al., 1992). Thus, a lateral resolution of $3.1nm$ easily meets our requirement for being able to stimulate single synapses. Our study requires patterned stimulation with the possibility of returning to previously stimulated synapses. The repeatability of the Canon galvo is $3\mu m$, which yields a possible error of $12nm$ at the sample (Eq. 10 & 11).

4 Complications and Future Direction

During early postnatal life, synapses in the LSO are selectively strengthened or weakened before hearing onset. We want to study the distribution of excitatory and inhibitory synapses on the LSO principal cell at early postnatal life, and how these inputs are redistributed over development. We use through-the-lens photouncaging as a direct method of mapping the distribution of these phenotypically different synapses. By passing our laser light through the objective lens of our microscope, we can focus our light to a spot size on the order of hundreds of nanometers. This

tight focus allows us to uncage a bolus of caged neurotransmitters small enough to stimulate a single synaptic input, and coupled with the extremely fast and precise galvo, we can reposition our light and stimulate synapses throughout an LSO principal neuron. In addition, we can program the galvo to plot deflection patterns uniformly across the FOV. The high angular resolution of the galvo allows us to precisely stimulate individual inputs without 'spillover' onto neighbouring synapses, giving a tight uncaging grid across the LSO principal neuron. Whole-cell patch clamp is used to record the electrical response of the LSO principal neuron after stimulation of a synaptic input. With this physiological data, we can produce a high-resolution map of these inhibitory and excitatory inputs over development.

4.1 Reasoning for UV Laser

UV light is not ideal for many photouncaging applications. It provides high resolution uncaging when passed through the lens but it is extremely phototoxic to living tissue. Two-photon uncaging is the ideal approach for our photouncaging experimentation for several reasons: 1) It is not phototoxic to our tissue sample; 2) we can achieve deeper tissue penetration; and 3) uncaging is confined to the focal plane of the objective (see Section 2.3). In light of budget constraints and the core similarities between one- and two-photon systems, the decision was to build a one-photon system that would make a subset of experiments possible, and later to modify this system for two-photon uncaging. Modifying this system for two-photon uncaging will require – in addition to the acquiring a femtosecond laser – replacing UV-optimized optical parts (mirrors, beam expander, scan lens, etc) with parts graded for NIR wavelengths. We will need to do the same calculations as in Section 3.3, but the wavelength component will be changed. The most difficult part of this modification will be re-aligning the newly added NIR graded components. Below, I provide a design for a two-photon system, including the relevant calculations and parts required.

4.2 Future Avenues: Two-Photon Uncaging

System Specifications

Please refer to Section 3.3 to see the specifications of our Olympus BX51 microscope. One attractive option for a fixed-wavelength laser in the two-photon system is a $780nm$ femtosecond laser (Toptica Photonics Femtofiber Pro NIR, New York) with a $1.5mm$ laser beam diameter. The transmissivity of our Olympus objective (Olympus LUMPLFLN 40XW) is approximately 83% in the $780nm$ wavelength. This objective lens is more suited for NIR transmission than UV. The f-theta scan lens (Thorlabs LSM54-850, New Jersey) is graded for approximately 93% transmissivity in wavelengths between $750 - 850nm$ and has an effective focal length of $54mm$. It can focus a maximum beam diameter of $6mm$ to a minimum spot size of $14\mu m$ within a scanning range of $\pm 14°$. The Canon GM-1010 galvo scanner has a reflectivity of above 95% in the $780nm$ wavelength, far superior to its reflectivity in the UV. For the other specification of the Canon galvo, refer to Section 3.3. For redirecting the NIR laser light, our UV mirrors will not be efficient. We will therefore use NIR graded mirrors from Thorlabs which are manufactured for use with femtosecond lasers (Thorlabs UM05-AG, New Jersey).

NIR Femtosecond Laser

Two-photon uncaging requires an ultra-fast, NIR or IR femtosecond laser. These lasers range in price from $\$60,000 - \$200,000$ CND depending on whether they have a fixed wavelength or are tunable. The FemtoFiber Pro NIR, manufactured by Toptica Photonics is our femtosecond laser of choice for a fixed wavelength femtosecond laser. It is a $140mW$, $780nm$ wavelength laser with less than $100fs$ pulses. This is considered a high-powered laser, and NIR laser safety glasses (Thorlabs LG12 Laser Safety Glasses, New Jersey) should be worn. The black-out boards and curtains in place for the UV laser will be kept up for the femtosecond laser as well. For other safety precautions refer to Section 3.2.

The probability of a two-photon absorption event is low (Section 2.3). To maximize the absorption efficiency, we want to maximize the laser intensity at the sample. We do this by keeping our laser power high and focusing our laser light to a small spot at the sample (Section 2.2). NDFs is used to control our NIR laser, no differently than with our UV laser. High-efficiency NIR mirrors (UM05-AG) will be used to contain the NIR laser beam within our table and direct the beam to the other optical components, including the galvo and microscope. We will need to purchase a dichroic mirror (Semrock NF03-785E-25, New York) graded for the $780nm$ wavelength, and it is used the same way as the UV graded dichroic mirror (Section 3.2).

Scan Lens Requirements

As mentioned before, we must ensure the specifications of our scan lens meet those of our objective lens. The resolution of our objective lens is $595nm$ at $780nm$ (Eq. 8). This is the theoretical limit of our uncaging spots in the NIR. The resolution seen at the conjugate plane is $23.8\mu m$ in the NIR (Eq. 12). The Thorlabs scan lens supports a minimum spot size of $14\mu m$ allowing us to

obtain this theoretical uncaging spot diameter of $595nm$. Based on the best available information, we expect this resolution will be sufficient to uncage individual synapses onto LSO principal neurons (Helfert et al., 1992). The numerical aperture at the scan lens needed to acquire a spot size of $23.8\mu m$ is 0.02 (Eq. 8), and the beam diameter required for this numerical aperture is $2.2mm$ (Eq. 13). This beam diameter fits within the range of our scan lens and galvo. In this situation (unlike with the Lenstek UV scan lens), the Thorlabs scan lens can focus our light tighter than the limits of our objective. By slightly tightening our focus at the scan lens, focusing our light to smaller than $23.8\mu m$ in diameter, we can capture more of the intensity profile of the laser light. This will not increase the resolution we see at the sample as the objective lens ultimately dictates our resolution limits. A NIR beam expander (Thorlabs BE052-B, New Jersey) will be used to magnify our $1.5mm$ laser beam to a little over $2.2mm$.

Galvanometer Requirements

As mentioned in Section 3.3, the performance of the galvos is affected by the scan lens. The Thorlabs' scanning lens allows for a scanning angle of $\pm 14°$ which limits our galvo scanning range. This limitation of the scan lens gives us a lateral scanning field of $330\mu m \times 330\mu m$ at the sample. This is smaller than the objective lens' FOV but is sufficient to cover the full dendritic field of the typical LSO principal neuron (Eq. 10 & 11; Rietzel and Friauf, 1998). The angular resolution of the Canon galvo is $0.77\mu rad$ which translates to a lateral resolution of $1nm$ at the sample (Eq. 10 & 11). This lateral resolution is sufficient to stimulate synapses onto an LSO principal neurons without stimulating neighbouring synapses (Helfert et al., 1992). The repeatability of the galvo, $3\mu m$, results in an error of $4nm$ at the sample (Eq. 10 & 11) which would not cause accidental stimulation of an adjacent synapse.

One-photon and two-photon photouncaging system have many similarities. With the modular nature of the set-up, our one-photon system can be converted quite easily to a two-photon one (Table 2).

4.3 Moving Forward

With the design and parts in hand, the next step is to assemble, and align the optical system. The design and groundwork presented is sufficient for a future lab member to finish the one-photon uncaging system.

There are many online resources that help with understanding the basics of microscopy. These basics include ray tracing, image formation and lens optics. Understanding these concepts will help get the best performance out of the optics, while testing the limits of light microscopy. *iBiology* is a great online microscopy resource center with lectures explaining ray tracing, lens optics, image formation and much more.

McMaster University offers many laser optics courses in the Department of Engineering Physics. "ENGPHYS 3EO3 – Fundamentals of Physical Optics," is an introductory course for understanding the principles of electromagnetic waves, light interference, optical properties of materials, introduction to optical systems and more. This course is followed by "ENGPHYS 4SO3/6S03 – The Introduction to Lasers and Electro-Optics," which covers the basic properties of light in terms of electro-magnetic fields. The course also explains concepts of geometric and physical optics, the propagation of light through materials and the basics of non-linear optics. Finally, the course covers the basics of lasers and laser operations in the context of a laser system (laser, optical mirrors, detectors, modulators, fibre optics and more). "ENGPHYS 4I03 – Introduction to Biophotonics," is a great

introductory course applying the concepts of light optics to biological applications. This includes light interactions with biological systems, and the use of photonics in biomedical applications.

The student who takes over this project may find the review by Svoboda and Yasuda (Svoboda and Yasuda, 2006) and the methods paper by Sarkisov and Wang (Sarkisov and Wang, 2007) especially helpful.

McMaster University is home to many laser optics labs. Collaboration with Dr. Qiyin Fang's lab will prove to be beneficial when it comes time to aligning the optical system.

One-photon Design			Two-photon Design		
Component	Part	Price (USD)	Component	Part	Price (USD)
Laser Source	DPSS Series 3500 UV Laser	$28,000.00	Laser Source	Toptica FemtoFiber Pro NIR	$45,000.00
Dielectric Mirrors	Thorlabs BB05	$88.49 (each)	Ultrafast-Enhanced Mirrors	Thorlabs UM05-AG	$62.48 (each)
Variable Beam Expander	Lenstek BX-Z-355-2-8X	$680.00	Variable Beam Expander	Thorlabs BE052-B	$847.62
Mirror Galvanometer	Canon GM-1010	$10,900.00	Mirror Galvanometer	Canon GM-1010	$10,900.00
Scanning Lens	Lenstek FL-355-112-160	$750.00	Scanning Lens	Thorlabs LSM54-850	$1564.68
Dichroic Mirror	ChromaTech 380dcip	$519.00	Dichroic Mirror	Semrock NF03-785E-25	$1280.00
Objective Lens	Olympus LUMPLFLN 40XW	$3357.00	Objective Lens	Olympus LUMPLFLN 40XW	$3357.00
	Total:	$44,366.49		Total:	$63,011.78

Table 2: Table showing the modular nature of the optical designs. One-photon design components and their analogous two-photon design components are listed along with their part ID and price.

5 Concluding Remarks

Development of the sound localizing circuitry in the auditory brainstem is crucial for organisms in understanding the world around them. This circuitry undergoes refinement, and this refinement is believed to occur functionally and anatomically, and it is believed to be activity-dependent. The neural activity involved with refinement is not fully understood but we know the patterned activity results in the release of GABA/glycine for the MNTB-LSO pathway, and glutamate for the AVCN-LSO pathway.

Off-the-shelf photouncaging solutions are expensive, annd are not always modifiable by the user. With through-the-lens uncaging, we can achieve near-diffraction limited stimulation by passing the light through the microscope's objective lens. Coupling our photostimulation with electrophys-

iological recording, we can map out the locations of synaptic inputs onto an LSO principal neuron and the strength of the input as a function of position. Through-the-lens photouncaging will help us study the activity-dependent refinement in the MNTB-LSO and AVCN-LSO pathways.

6 References

Adams SR, Tsien RY (1993) Controlling cell chemistry with caged compounds. Annu Rev Physiol 55:755–784.

Benninger RKP, Piston DW (2013) Two-Photon Excitation Microscopy for the Study of Living Cells and Tissues. Curr Protoc Cell Biol 0 4:Unit-4.1124.

Bledsoe S, Snead C, Helfert R, Prasad V, Wenthold R, Altschuler R (1992) Immunocytochemical and lesion studies support the hypothesis that the projection from the medial nucleus of the trapezoid body to the lateral superior olive is glycinergic. Brain Research 517:189–194.

Boudreau JC, Tsuchitani C (1968) Binaural interaction in the cat superior olive S segment. J Neurophysiol 31:442–454.

Case DT, Zhao X, Gillespie DC (2011) Functional Refinement in the Projection from Ventral Cochlear Nucleus to Lateral Superior Olive Precedes Hearing Onset in Rat PLoS ONE 6:e20756.

Clause A, Kim G, Sonntag M, Weisz CJC, Vetter DE, Rűbsamen R, Kandler K (2014) The precise temporal pattern of prehearing spontaneous activity is necessary for tonotopic map refinement. Neuron 82:822–835.

Ellis-Davies GCR (2007) Caged compounds: photorelease technology for control of cellular chemistry and physiology. Nat Methods 4:619–628.

Ellis-Davies GCR (2011) Two-Photon Microscopy for Chemical Neuroscience. ACS Chem Neurosci 2:185–197.

Fino E, Araya R, Peterka DS, Salierno M, Etchenique R, Yuste R (2009) RuBi-Glutamate: Two-Photon and Visible-Light Photoactivation of Neurons and Dendritic spines. Front Neural Circuits 3

Galli L, Maffei L (1988) Spontaneous impulse activity of rat retinal ganglion cells in prenatal life. Science 242:90–91.

Glendenning KK, Masterton RB, Baker BN, Wenthold RJ (1991) Acoustic chiasm III: Nature, distribution, and sources of afferents to the lateral superior olive in the cat. J Comp Neurol 310:377–400.

Grothe B, Pecka M, McAlpine D (2010) Mechanisms of Sound Localization in Mammals. Physiological Reviews 90:983–1012.

Helfert RH, Juiz JM, Bledsoe SC, Bonneau JM, Wenthold RJ, Altschuler RA (1992) Patterns of glutamate, glycine, and GABA immunolabeling in four synaptic terminal classes in the lateral superior olive of the guinea pig. J Comp Neurol 323:305–325.

Ikrar T, Olivas ND, Shi Y, Xu X (2011) Mapping Inhibitory Neuronal Circuits by Laser Scanning Photostimulation. Journal of Visualized Experiments

Kandler K, Gillespie DC (2005) Developmental refinement of inhibitory sound-localization circuits. Trends in Neurosciences 28:290–296.

Kandler K, Nguyen T, Noh J, Givens RS (2013) An Optical Fiber-Based Uncaging System. Cold Spring Harb Protoc 2013:118–121.

Kantevari S, Matsuzaki M, Kanemoto Y, Kasai H, Ellis-Davies GCR (2010) Two-color, two-photon uncaging of glutamate and GABA. Nat Methods 7:123–125.

Katz L, Shatz C (1996) Synaptic activity and the construction of cortical circuits. Science 274:1133–1138.

Kim G, Kandler K (2003) Elimination and strengthening of glycinergic/GABAergic connections during tonotopic map formation. Nat Neurosci 6:282–290.

Korada S, Schwartz IR (1999) Development of GABA, glycine, and their receptors in the auditory brainstem of gerbil: a light and electron microscopic study. J Comp Neurol 409:664–681.

Kotak VC, Korada S, Schwartz IR, Sanes DH (1998) A developmental shift from GABAergic to glycinergic transmission in the central auditory system. J Neurosci 18:4646–4655.

Liang CW, Mohammadi M, Santos MD, Tang C-M (2011) Patterned Photostimulation with Digital Micromirror Devices to Investigate Dendritic Integration Across Branch Points. J Vis Exp

Matsuzaki M, Ellis-Davies GC, Nemoto T, Miyashita Y, Iino M, Kasai H (2001) Dendritic spine geometry is critical for AMPA receptor expression in hippocampal CA1 pyramidal neurons. Nat Neurosci 4:1086–1092.

Meister M, Wong R, Baylor D, Shatz C (1991) Synchronous bursts of action potentials in ganglion cells of the developing mammalian retina. Science 252:939–943.

Momotake A, Lindegger N, Niggli E, Barsotti RJ, Ellis-Davies GCR (2006) The nitrodibenzofuran chromophore: a new caging group for ultra-efficient photolysis in living cells. Nat Methods 3:35–40.

Moore MJ, Caspary DM (1983) Strychnine blocks binaural inhibition in lateral superior olivary neurons. J Neurosci 3:237–242.

Nabekura J, Katsurabayashi S, Kakazu Y, Shibata S, Matsubara A, Jinno S, Mizoguchi Y, Sasaki A, Ishibashi H (2004) Developmental switch from GABA to glycine release in single central synaptic terminals. Nat Neurosci 7:17–23.

Penn AA, Riquelme PA, Feller MB, Shatz CJ (1998) Competition in retinogeniculate patterning driven by spontaneous activity. Science 279:2108–2112.

Rial Verde EM (2008) Photorelease of GABA with visible light using an inorganic caging group.

Frontiers in Neural Circuits 2

Richers MT, Amatrudo JM, Olson JP, Ellis-Davies GCR (2017) Cloaked Caged Compounds: Chemical Probes for Two-Photon Optoneurobiology. Angew Chem Int Ed Engl 56:193–197.

Rietzel H, Friauf E (1998) Neuron types in the rat lateral superior olive and developmental changes in the complexity of their dendritic arbors. The Journal of Comparative Neurology 390:20–40.

Römer GRBE, Bechtold P (2014) Electro-optic and Acousto-optic Laser Beam Scanners. Physics Procedia 56:29–39.

Russell A, Moore D (1995) Afferent reorganisation within the superior olivary complex of the gerbil: Development and induction by neonatal, unilateral cochlear removal. J Comp Neurol 352:607–625.

Sanes DH, Geary WA, Wooten GF, Rubel EW (1987) Quantitative distribution of the glycine receptor in the auditory brain stem of the gerbil. J Neurosci 7:3793–3802.

Sanes DH, Rubel EW (1988) The ontogeny of inhibition and excitation in the gerbil lateral superior olive. J Neurosci 8:682–700.

Sarkisov DV, Wang SS-H (2007) Combining Uncaging Techniques with Patch-Clamp Recording and Optical Physiology. In: Patch-Clamp Analysis, pp 149–168 Neuromethods. Humana Press

Shembekar VR, Chen Y, Carpenter BK, Hess GP (2007) Coumarin-caged glycine that can be

photolyzed within 3 microseconds by visible light. Biochemistry 46:5479–5484.

Shepherd GMG, Svoboda K (2005) Laminar and columnar organization of ascending excitatory projections to layer 2/3 pyramidal neurons in rat barrel cortex. J Neurosci 25:5670–5679.

Svoboda K, Yasuda R (2006) Principles of two-photon excitation microscopy and its applications to neuroscience. Neuron 50:823–839.

Tritsch N, Yi E, Gale J, Glowatzki E, Bergles D (2007) The origin of spontaneous activity in the developing auditory system. Nature 450:50–55.

Tritsch NX, Bergles DE (2010) Developmental regulation of spontaneous activity in the Mammalian cochlea. J Neurosci 30:1539–1550.

Ueno S, Nabekura J, Ishibashi H, Akaike N, Mori T, Shiga M (1995) Photolysis of a newly synthesized caged glycine activates the glycine receptor of rat CNS neurons. J Neurosci Methods 58:163–166.

Wu SH, Kelly JB (1992) Synaptic pharmacology of the superior olivary complex studied in mouse brain slice. J Neurosci 12:3084–3097.

Zeng S, Luo Q, Li D, Lü X (2009) Femtosecond pulse laser scanning using Acousto-Optic Deflector. Sci China Ser G-Phys Mech Astron 52:685.

Zhu P, Fajardo O, Shum J, Zhang Schärer Y-P, Friedrich RW (2012) High-resolution optical control of spatiotemporal neuronal activity patterns in zebrafish using a digital micromirror device. Nat Protoc 7:1410–1425.